T. Yumak / Hacettepe J. Biol. & Chem., 2019, 47 (1), 115–122

Research Article

Hacettepe Journal of Biology and Chemistry

journal homepage: www.hjbc.hacettepe.edu.tr

Electrochemical Performance of Fabricated Supercapacitors Using MnO_2/Activated Carbon Electrodes

MnO_2/Aktif Karbon Elektrotlar ile Üretilen Süperkapasitörlerin Elektrokimyasal Performansı

Tuğrul Yumak

Department of Chemistry, Sinop University, Sinop, Turkey.

ABSTRACT

Peanut shells were subjected to pyrolysis and chemical activation to produce activated carbon with high specific surface area. MnO_2 particles were synthesized on the activated carbon surface. Supercapacitors were fabricated by using activated carbon electrodes and tested by constant current charge-discharge, self-discharge, and life-cycle tests. MnO_2 loading led to a significant decrease in specific surface area. The pore volume distribution calculations revealed that the MnO_2 particles were in nanometer size. Because of the reduction of MnO_4^- Ions to MnO_2 over the activated carbon surface, the amount of oxygen-containing surface functional groups, changed. Although the MnO_2 loading caused a decrease in surface area, the specific capacitance increased from 49 F/g to 68 F/g.

Keywords

EDLC, fabrication of supercapacitor, electrochemical testing of supercapacitors, activated carbon.

ÖZ

Fıstık kabuklarından piroliz ve kimyasal aktivasyon teknikleri kullanılarak yüksek yüzey alanına sahip aktif karbon üretilerek, bu aktif karbonun yüzeyinde MnO_2 sentezlendi. Aktif karbonlar elektrot olarak kullanılarak süperkapasitörler fabrike edildi ve sabit akım şarj-deşarj, kendiliğinden boşalma ve çevrim ömrü testleri gerçekleştirildi. MnO_2 yüklemesi yüzey alanında azalmaya yol açmıştır. Gözenek hacim dağılımı hesaplamaları sentezlenen MnO_2 parçacıklarının nanometre boyutunda olduğunu göstermiştir. MnO_4^- iyonlarının aktif karbon yüzeyinde MnO_2'ye yükseltgenmesi nedeni ile yüzeyde oksijen içeren fonksiyonlu grupların sayısında değişim olmuştur. MnO_2 yüklemesi yüzey alanı düşüşüne sebep olmasına rağmen, spesifik kapasitansın 49 F/g'dan 68 F/g'a çıkmasına yol açmıştır.

Anahtar Kelimeler

EDLC, süperkapasitör üretimi, süperkapasitörlerin elektrokimyasal testleri, aktif karbon.

Article History: Received: Dec 30, 2018; Revised: Jan 08, 2019; Accepted: Jan 17, 2019; Available Online: Mar 01, 2019.

DOI: 10.15671/HJBC.2019.281

Correspondence to: T. Yumak, Department of Chemistry, Sinop University, Sinop, Turkey.

E-Mail: tyumak@sinop.edu.tr

INTRODUCTION

Carbon materials are widely used in water purification [1,2], gas storage [3], catalyst support for gas-solid reactions [4], and electrochemical applications [5] due their relatively low cost and versatile existing forms such as powders, fibers, felts, composites, mats, monoliths, and foils [6]. Additionally, the ease of processability, relatively inert electrochemistry, controllable porosity and electrocatalytic active sites for a variety of redox reactions make the activated carbons one of the desired materials for electrochemical double layer capacitor (EDLC) applications (supercapacitors) [7]. As the activated carbons are electrochemically inactive, no electrochemical reaction takes place on the electrode and energy stored by pure physical accumulation at the electrode/electrolyte interface [8]. However, they suffer from poor energy storage capacity and inferior rate capability [9]. Therefore, the physicochemical properties of activated carbons should be improved in order to fabricate higher capacitive performance supercapacitors. Physical or chemical activation of activated carbons can be possessed as an option to control the pore characteristics and increase the surface area [10]. It is reported that the physical activation leads to narrower pore size distributions while chemical activation is more effective on the higher packing density and bringing about a positive effect on the volumetric adsorption capacity [11]. One other option may be the combining carbon materials with either metal oxides or conducting polymers to improve the capacitive performance through the synergistic effect of both EDLC and pseudocapacitance mechanisms [12]. Recent studies showed that the MnO_2 and NiO loading on the activated carbon led to a significant increase in capacitive performance of fabricated symmetrical activated carbon-based supercapacitors [13,14]. Moreover, both activation and metal oxide loading lead to an increase in the oxygen-containing surface functional groups, which may enhance the wettability of the electrode surface, and create additional pseudocapacitance via redox reactions during the charge/discharge process.

Various measuring methods such as cyclic voltammetry (CV), galvanostatic and constant current charge-discharge, external resistor discharge and impedance spectroscopy, currently being employed to determine the capacitive performance. However, there is not a widely accepted standard to determine and compare the capacitive performance of supercapacitors [15]. Most of the reported results used CV technique in three or two electrode system while only a few works concerned with the packaged cells. Although it is reported that two-electrode cells allow a good estimation of materials performance in supercapacitors [16], the real capacitive performance of the packaged cell is much smaller due to the cell architecture, electrolyte amount and ion transfer through the membrane issues. Therefore, in this study, the effect of the MnO_2 loading on the real capacitive performance of a chemically activated carbon-based packaged symmetrical supercapacitor was investigated. First, the activated carbon was prepared by the H_3PO_4 activation of pre-carbonized peanut shells at 800°C, and then MnO_2 were loaded on the as-synthesized activated carbon via precipitation. Afterward, the electrodes were prepared by a casting technique and the supercapacitors were assembled in CR2032 casings. N_2 physisorption was used to determine the surface area and NLDFT (Non Localized Density Functional Theory) was applied to adsorption isotherms in order to state the pore volume distribution. Raman and XPS were used to discuss the effect of MnO_2 loading on a surface and chemical structure of chemically activated carbon. The specific capacitance and the self-discharge behavior of the fabricated supercapacitors were determined by constant current discharge technique.

MATERIALS and METHODS

Preparation of Electrode Materials

The peanut shells were ground to very fine dust and then sieved (400 mesh). The obtained powders were pyrolyzed for 30 min at 600°C before the chemical activation step. H_3PO_4 (CAS Number 7664-38-2, ACROS) activation was conducted at 800°C for 1 h. N_2 inert atmosphere was used in both pyrolysis and activation at a flow rate of 10 mL/min. The collected powders after activation were washed with hot distilled water, followed by drying in 105°C oven for 24 h. Finally, the obtained material was denoted as H_3PO_4-AC. $KMnO_4$ (CAS Number 7722-64-7, ACROS) was used as Mn source and the loading procedure was described in a previous study [14]. After the precipitation of MnO_2 and drying process, the obtained material was donated as MnO_2/H_3PO_4-AC.

Fabrication of Electrodes and Supercapacitors

The electrode mixture was prepared by mixing activated carbon (AC) (H_3PO_4-AC or MnO_2/H_3PO_4-AC), carbon black (CB) (CAS Number 1333-86-4, Alfa Aesar),

Poly(tetrafluoroethylene) (PTFE) (CAS Number 9002-84-0, ACROS) and adequate amount of N-Methyl-2-Pyrrolidone (NMP) (CAS Number 872-50-4, ACROS), the weight ratio of AC:CB:PTFE is 85:5:10. The mixture was stirred for 24 h and casted on SS304 plate with 0.60 mm thickness. After complete drying, the electrodes (ø=13 mm) and filter paper (ø=15 mm) were punched and soaked in 6M KOH (CAS Number 1310-58-3, ACROS) for 24h. Supercapacitors were assembled in CR2032 casings and sealed by a hand press.

Materials Characterization and Electrochemical Testing

The synthesized carbon materials were characterized by N_2 Physisorption and NLDFT to determine the surface area and pore volume distribution. N_2 adsorption-desorption isotherms were obtained by Micromeritics 3Flex volumetric gas adsorption based on HK83 points method at 77 K. Raman and XPS were used in order to determine the chemical structure and surface chemistry, as well as surface functional groups. Raman spectra was recorded by WITec alpha300 Series with 532 nm Ar laser excitation. Specs-Flex was used for x-ray photoelectron spectroscopy studies using Al Kα (1486.6 eV) radiation, survey scan with a 0.5 eV step and detailed scan with a 0.05 eV. Adventitious carbon (C1s) peak at 284.5 eV used as the reference. The electrochemical testing of the fabricated supercapacitors was conducted on the Gamry Reference 1010(E) as outlined in supercapacitor testing standard IEC 62391-1:2006. The self-discharge behavior for 50 cycles and constant current charge-discharge tests for 1000 cycles was performed in a voltage range of 0.1V to 1 V with a constant current density of 0.1 A/g. The gravimetric specific capacitance of the supercapacitors was calculated from Eq. (1) after excluding the ohmic part, equivalent series resistance (ESR).

$$\frac{C_g}{Fg^{-1}} = \frac{2l}{(dV/dt)m} \quad (1)$$

where Cg represents the gravimetric specific capacitance, I is the discharge current, m is the average mass of one electrode, and dV/dt is the rate of voltage change.

RESULTS and DISCUSSION

The adsorption/desorption isotherms of H_3PO_4-AC and MnO_2/H_3PO_4-AC powders and the cumulative pore volume distribution from adsorption isotherms by applying a hybrid nonlocal DFT (NLDFT) kernel, assuming a slit-shaped pore for the micropores and a cylindrical pore for the mesopores are shown in Figure 1. Both samples display a Type-IV adsorption isotherm, which is typical of mesoporous materials [17]. A clear step at 0.4-0.6 relative pressures indicates the uniform mesoporous structure [18]. However, the typical H4 loops for micro-mesoporous carbons [17] shows the formation of microporous structure also. Similar isotherms were observed indicating that the MnO_2 loading did not affect the pore characteristics of H_3PO_4 activated of biomass-derived carbon. The surface area of H_3PO_4-AC and MnO_2/H_3PO_4-AC samples are 628.19 m^2/g and 336.45 m^2/g, respectively. The pore volume distribution showed that the synthesized materials consist of mostly micropores. The decrease in the pore volume is attributed to the formation of MnO_2 particles in the internal portion of the pores. The higher decrease in the micropore regime (pore size < 2 nm)

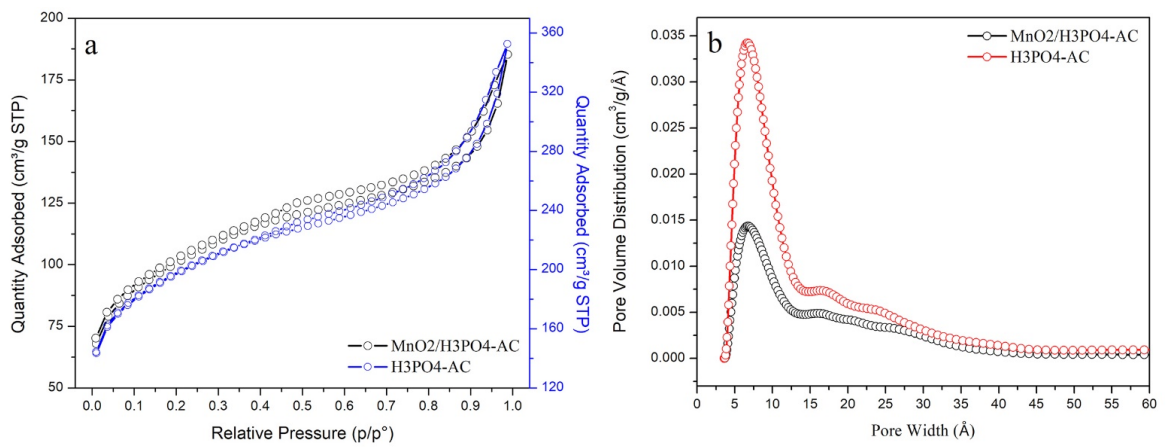

Figure 1. a) N_2 physisorption isotherms and b) calculated pore volume distribution of H_3PO_4-AC and MnO_2/H_3PO_4-AC powders.

compared to the mesopore regime (2 nm < pore size < 50 nm) may suggest the formation of nanometer-sized MnO_2 particles.

Raman spectroscopy is one of the most useful technique to characterize carbon-based materials because the spectral shape is highly sensitive to the fine structural changes of the material. Figure 2 shows the Raman spectra and deconvolution of the spectra into two Gaussians. As seen in the figure, the typical G band (1500-1600 cm^{-1}) and D band (1300-1400 cm^{-1}) for heterogeneous carbon microstructure were observed. The overlap without a clear separation between G and D bands is evidence for disordered activated carbons [19]. The G band is related to the to E_{2g} graphite mode while the D band is attributed to the defective structures [20]. An increase in the I_D/I_G ratio was observed with MnO_2 loading indicating the disorder of the sample is increased. In addition, MnO_2 loading caused a blue shift (9 cm^{-1}) was observed in G band which may be attributed to the charge transfer between the carbon and MnO_2 species [21,22]. Moreover, two different parts of the MnO_2/H_3PO_4-AC sample were investigated. In the first part, peaks were observed at around 500-650 cm^{-1} indicating the presence of MnO_2. However, these peaks are overlapped and very complicated. In the second part, there was no peak related to the presence of MnO_2. These two opposite situations suggest that the distribution of MnO_2 on the activated carbon is not homogenous.

The surface composition and chemical states of the elements were determined by XPS analysis. Figure 3 shows the deconvolution O1s peaks and Mn2p peak of as-synthesized materials. In the O1s spectra (Figure 3a and b), two main peaks corresponding to the C=O (oxygen doubly bonded to aromatic carbon) at ≈531 eV, and C–O (oxygen singly bonded to aliphatic carbon) at ≈532 eV [23,24] were observed. The MnO_2/H_3PO_4-AC sample consists of two peaks centered at 641.20 and 652.93 eV (Figure 3c), which correspond to the binding energies of Mn $2p_{3/2}$ and Mn $2p_{1/2}$ of Mn^{4+} oxidation states [25]. It is obvious that the MnO_2 loading caused a narrower O1s peak shape and relative increase in C=O groups ratio on the surface. Since

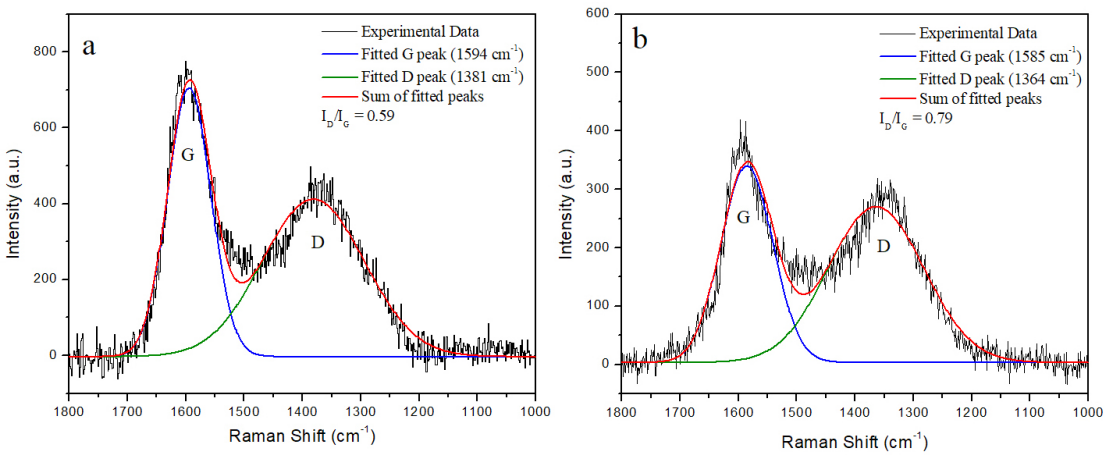

Figure 2. a) Deconvolution of the Raman spectra of a) H_3PO_4-AC and b) MnO_2/H_3PO_4-AC powders.

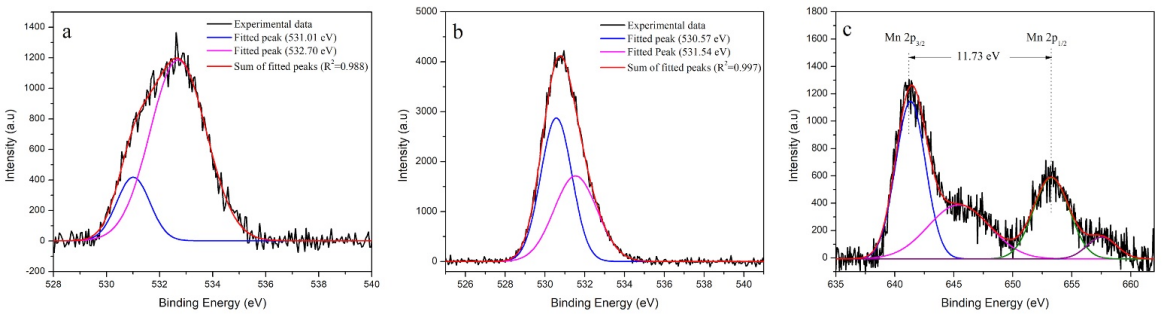

Figure 3. a) Deconvolution of the O1s spectra of a) H_3PO_4-AC and b) MnO_2/H_3PO_4-AC and c) Mn 2p spectra of MnO_2/H_3PO_4-AC.

the reductive effect of activated carbon is responsible for the reduction of MnO_4 to MnO_2 [26], it may be said that the C-O groups are more effective than the C=O groups for the reduction of $KMnO_4$. The atomic and weight concentration of Mn in the MnO_2/H_3PO_4-AC sample is found to be 2.09% and 7.37%.

The constant current charge-discharge (CCD) curves and self-discharge behavior of supercapacitors fabricated by using H3PO4-AC and MnO2/H3PO4-AC as symmetrical electrodes are shown in Figure 4. The constant current charge-discharge and self-discharge tests were performed at a current density of 0.1 A/g and 0.1-1 V voltage window due to the standard potential of water electrolysis (1.23 V). The charge-discharge curves represent very cyclic behavior for both samples. They showed the typical symmetrical triangular shape indicating a high-rate capacitive performance [27]. However, the perfect triangle shape was slightly distorted by the MnO_2 loading due to the higher ESR. Furthermore, the adsorption-desorption capacity of the electrode which is highly influenced by the surface area may also be responsible for the distortion. The ESR drop for the H_3PO_4-AC and MnO_2/H_3PO_4-AC based fabricated supercapacitors was 0.09 V and 0.16 V, respectively. The higher ESR drop may be related to the decrease in the mobility of the ions on the electrodes [27]. The redox reactions over the MnO_2 in the MnO_2/H_3PO_4-AC electrode may affect the mobility of the ions.

The self-discharge behavior of a supercapacitor is an important factor in determining the capability of charge holding and the performance. The self-discharge can be explained by activation-controlled Faradaic process, diffusion-controlled Faradaic redox reactions and internal

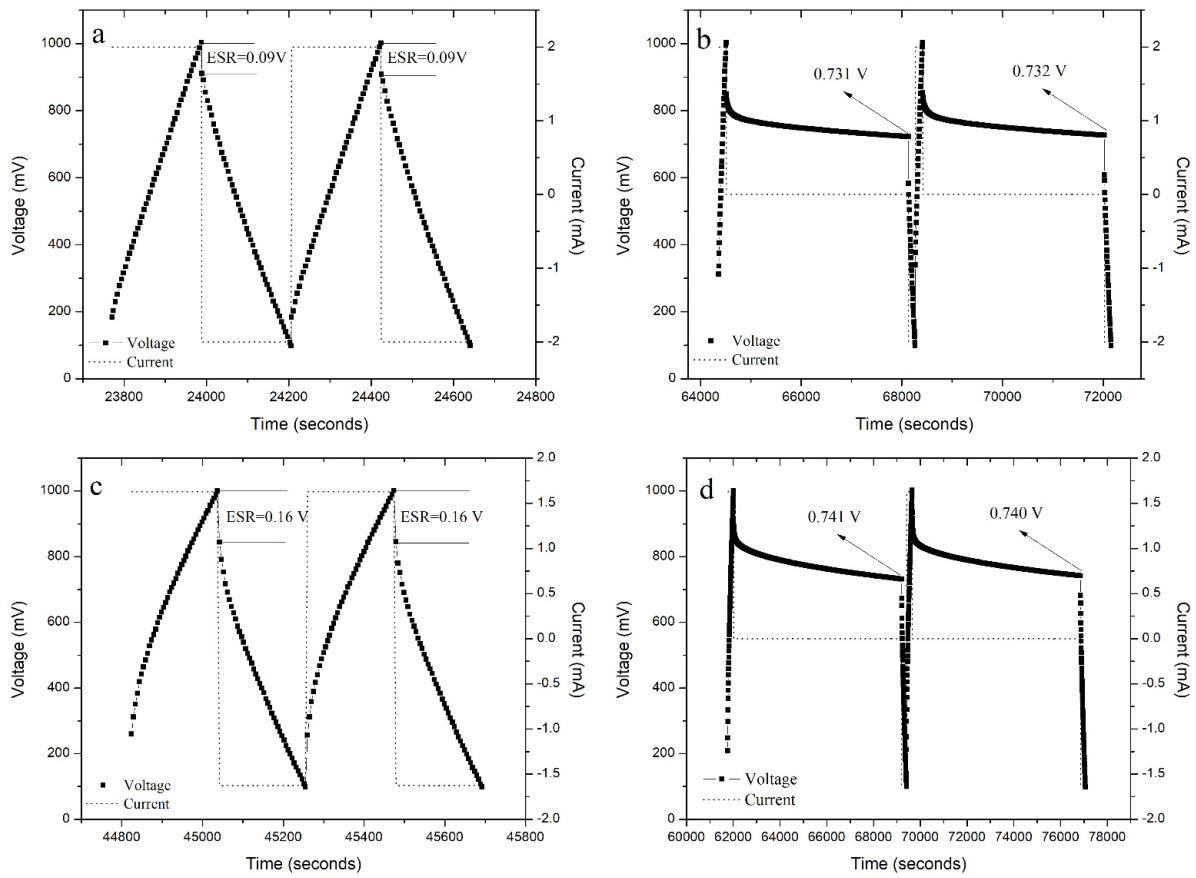

Figure 4. a) Constant current charge-discharge curves of a) H_3PO_4-AC and c) MnO_2/H_3PO_4-AC; self-discharge behavior of b) H_3PO_4-AC and d) MnO_2/H_3PO_4-AC.

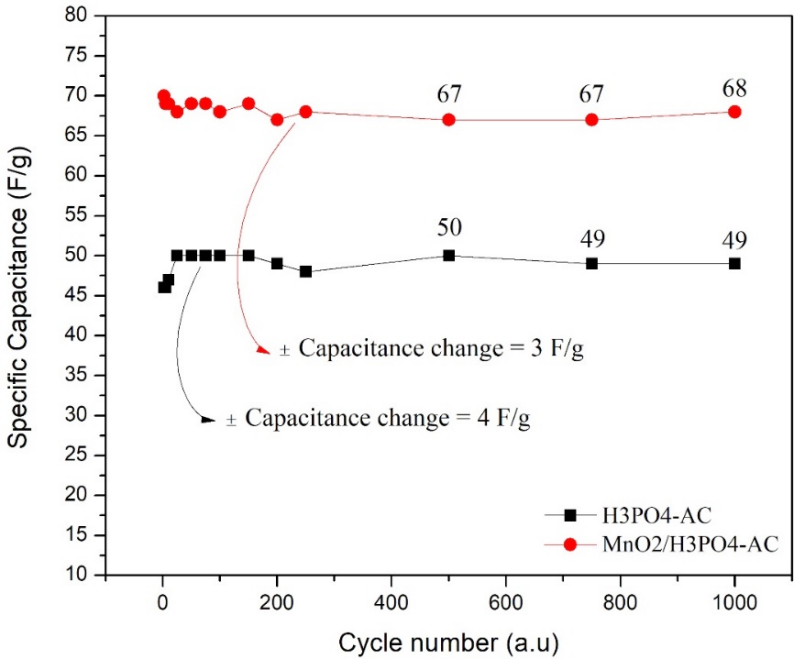

Figure 5. Specific capacitance change of fabricated supercapacitors over 1000 cycles.

ohmic leakage mechanisms [28]. The cell architecture may also affect the leakage. The self-discharge behavior of fabricated supercapacitors were calculated from the 49th and 50th cycle of the test are shown in Figure 4b and d. Almost similar self-discharge character after 120 min rest time was observed. The voltage loss is 0.27 V and 0.26 V for H_3PO4-AC and MnO_2/H_3PO_4-AC and did not vary more than 1% after 50 cycles indicating that the electrochemical performance of the fabricated supercapacitors was highly stable.

Figure 5 shows the specific capacity (Cg) at 0.1 A/g current density calculated from the discharge curves after excluding the IR drop. The Cg of the fabricated supercapacitors is 49 F/g and 68 F/g over 1000 cycles for H_3PO_4-AC and MnO_2/H_3PO_4-AC, respectively. The capacitance change during 1000 cycles is not more than 3-4 F/g indicating that the supercapacitors were highly stable. Although the MnO_2 loading caused a significant decrease in the specific surface area, the specific capacitance increase from 49 F/g to 68 F/g. This is attributed to the charge storage by redox reactions over MnO_2 species during the charge-discharge process. The redox reaction can be expressed as follows in Equation 2.

$$MnO_2 + K^+ + e^- \rightleftharpoons MnOOK \quad (2)$$

However, the charge storage mechanism is more complicated. The phase of the MnO_2 is influenced by the pH of the electrolyte. In this work, 6M KOH is used as electrolyte and after soaking process the electrodes were not dried. According to the Pourbaix diagram, the high pH of the environment will lead to the formation of Mn_2O_3 from MnO_2. In addition, Minakshi reported the formation of MnOOH after 50% discharge, and Mn_2O_3 and Mn_3O_4 after 100% discharge [29]. Therefore, the redox reaction between Mn_z^{2+}/Mn^{7+} species may be responsible for the charge storage. In situ XRD studies during the charge-discharge operation may be more effective to clarify the formation of Mn species and thus the charge storage mechanism.

As a result, high surface area activated carbon were produced by the pyrolysis and chemical activation. Nanometer-sized MnO_2 was formed on the activated surface by the precipitation method. $KMnO_4$ was reduced to MnO_2 via the hetero-atom containing surface functional groups over the activated carbon. Although the MnO2 loading caused a decrease in the specific surface area, the capacitive performance of the MnO_2/H_3PO_4-AC electrode increased. Moreover, the MnO_2 loading resulted in some changes in the chemical structure of the activated carbon surface. It can be said that not only the

pseudocapacitive effect of MnO_2 but also the changes in the surface chemistry is responsible for the performance increase. These results show that the peanut shell is a good candidate to produce activated carbon, and MnO_2 can be assessed as an effective pseudocapacitive material to increase the capacitive performance of activated carbon-based fabricated supercapacitors.

Acknowledgments

This work was supported by Sinop University Scientific Research Projects Coordination Unit through the Project Number, FEF-1901-16-13. Dr. Yumak also acknowledges the use of East Anatolia High Technology Application and Research Center (DAYTAM) for materials characterization.

References

1. E. Bayram, Electrosoption of aromatic organic acids from aqueous solutions onto granular activated carbon electrodes for water purification, Hacettepe J. Biol. Chem., 3 (2016) 273-273.
2. C. Haktanır, Removal of heavy metals from aqueus solution using activated carbon embedded cryogels, Hacettepe J. Biol. Chem., 1 (2017) 135-142.
3. S. Baş, Ö. Hakli, A.G. Dumanli, Y. Yürüm, PAN-based pd-doped activated carbon fibers for hydrogen storage : preparation , a new method for chemical activation and characterization of fibers, Hacettepe J. Biol. Chem. 36 (2008) 247-253.
4. H. Jüntgen, Activated carbon as catalyst support, Fuel, 65 (1986) 1436–1446.
5. R.W. Pekala, J.C. Farmer, C.T. Alviso, T.D. Tran, S.T. Mayer, J.M. Miller, B. Dunn, Carbon aerogels for electrochemical applications, J. Non. Cryst. Solids., 225 (1998) 74-80.
6. E. Frackowiak, Carbon materials for supercapacitor application., Phys. Chem. Chem. Phys., 9 (2007) 1774-785.
7. L.L. Zhang, X.S. Zhao, Carbon-based materials as supercapacitor electrodes, J. Mater. Chem. 38 (2009) 2520-2531.
8. G. Wang, L. Zhang, J. Zhang, A review of electrode materials for electrochemical supercapacitors, Chem. Soc. Rev. Chem. Soc. Rev., 41 (2012) 797-828.
9. S. Bose, T. Kuila, A.K. Mishra, R. Rajasekar, N.H. Kim, J.H. Lee, Carbon-based nanostructured materials and their composites as supercapacitor electrodes, J. Mater. Chem., 22 (2012) 767.
10. P.T. Williams, A.R. Reed, Development of activated carbon pore structure via physical and chemical activation of biomass fibre waste, Biomass and Bioenergy., 30 (2006) 144–152.
11. M.J. Prauchner, F. Rodríguez-Reinoso, Chemical versus physical activation of coconut shell: A comparative study, Microporous Mesoporous Mater., 152 (2012) 163-171.
12. M.Y. Ho, P.S. Khiew, D. Isa, T.K. Tan, a Review of metal oxide composite electrode materials for electrochemical capacitors, J. World Sci., 9 (2014) 1-25.
13. D. Deng, B.-S. Kim, M. Gopiraman, I.S. Kim, Needle-like MnO_2/activated carbon nanocomposites derived from human hair as versatile electrode materials for supercapacitors, RSC Adv., 5 (2015) 81492-81498.
14. T. Yumak, D. Bragg, E.M. Sabolsky, Effect of synthesis methods on the surface and electrochemical characteristics of metal oxide/activated carbon composites for supercapacitor applications, Appl. Surf. Sci. 469 (2019) 983-993.
15. M.D. Stoller, R.S. Ruoff, Best practice methods for determining an electrode material's performance for ultracapacitors, Energy Environ. Sci., 3 (2010) 1294-1301.
16. V. Khomenko, E. Frackowiak, F. Beguin, Determination of the specific capacitance of conducting polymer/nanotubes composite electrodes using different cell configurations, Electrochim. Acta., 50 (2005) 2499-2506.
17. M. Thommes, K. Kaneko, A.V. Neimark, J.P. Olivier, F. Rodriguez-Reinoso, J. Rouquerol, K.S.W. Sing, Physisorption of gases, with special reference to the evaluation of surface area and pore size distribution (IUPAC Technical Report), Pure Appl. Chem., 87 (2015) 1051-1069.
18. H. Peng, G. Ma, K. Sun, J. Mu, Z. Zhang, Z. Lei, Formation of carbon nanosheets via simultaneous activation and catalytic carbonization of macroporous anion-exchange resin for supercapacitors application, ACS Appl. Mater. Interfac., 6 (2014) 20795-20803.
19. K.C. Kemp, S. Bin Baek, W.G. Lee, M. Meyyappan, K.S. Kim, Activated carbon derived from waste coffee grounds for stable methane storage, Nanotechnology, 26 (2015).
20. J. Ma, Z. Zhu, B. Chen, M. Yang, H. Zhou, C. Li, F. Yu, J. Chen, One-pot, large-scale synthesis of magnetic activated carbon nanotubes and their applications for arsenic removal, J. Mater. Chem. A, 1 (2013) 4662-4666.
21. W. Huang, S. Ding, Y. Chen, W. Hao, X. Lai, J. Peng, J. Tu, Y. Cao, X. Li, 3D NiO hollow sphere/reduced graphene oxide composite for high-performance glucose biosensor, Sci. Rep., 7 (2017) 1-11.
22. Z. Wu, X.L. Huang, Z.L. Wang, J.J. Xu, H.G. Wang, X.B. Zhang, Electrostatic induced stretch growth of homogeneous β-Ni(OH)2on graphene with enhanced high-rate cycling for supercapacitors, Sci. Rep., 4 (2014) 1-8.
23. A. Ganguly, S. Sharma, P. Papakonstantinou, J. Hamilton, Probing the thermal deoxygenation of graphene oxide using high-resolution in situ X-ray-based spectroscopies, J. Phys. Chem. C, 115 (2011) 17009-17019.
24. S. Biniak, G. Szymanski, J. Siedlewski, A. Swiatkowski, The characterization of activated carbons with oxygen and nitrogen surface groups, Carbon N. Y., 35 (1997) 1799-1810.
25. X. Chang, X. Zhai, S. Sun, D. Gu, L. Dong, Y. Yin, Y. Zhu, MnO2/g-C3N4 nanocomposite with highly enhanced supercapacitor performance, Nanotechnology, 28 (2017) 135705-135714.
26. X. Dong, W. Shen, J. Gu, L. Xiong, Y. Zhu, H. Li, J. Shi, MnO_2-embedded-in-mesoporous-carbon-wall structure for use as electrochemical capacitors, J. Phys. Chem. B, 110 (2006) 6015-6019.
27. C. Zequine, C.K. Ranaweera, Z. Wang, P.R. Dvornic, P.K. Kahol, S. Singh, P. Tripathi, O.N. Srivastava, S. Singh, B.K. Gupta, G. Gupta, R.K. Gupta, High-performance flexible supercapacitors obtained via recycled jute: bio-waste to energy storage approach, Sci. Rep., 7 (2017) 1-12.

28. J.F. Shen, Y.J. He, Z.F. Ma, A systematical evaluation of olynomial based equivalent circuit model for charge redistribution dominated self-discharge process in supercapacitors, J. Power Sour., 303 (2016) 294-304.

29. M. Minakshi, Examining manganese dioxide electrode in koh electrolyte using TEM technique, J. Electroanal. Chem., 616 (2008) 99-106.